Metachronal propagation of motoneurone burst activation in isolated spinal cord of newborn rat

Jean-René Cazalets

CNRS UMR 5543, Université de Bordeaux II, Zone nord Bat 2, 2e étage, 146, rue Léo Saigna, 33076 Bordeaux cedex France

Adequate locomotor and postural activity in mammals results from the coordinated activation of assemblies of spinal cord networks. In order to assess the global functioning of spinal circuitry, multisite recordings were made from an isolated spinal cord preparation of the newborn rat. Motor activity, elicited in a disinhibited network by bath-applying strychnine (glycinergic blocker) and bicuculline (GABAergic blocker), consisted of slow spontaneous bursting. Under these conditions, the recorded bursts were coordinated in 1 : 1 relationships at all segmental levels. For each cycle, a leading segment initiated the activity that then propagated in a metachronal way through adjacent segments along the length of spinal cord. There was both regional non-linearity and directional asymmetry in this burst propagation: motor bursts propagated most rapidly in the thoracic spinal cord and the rostro-caudal wave travelled faster than the caudo-rostral one. Propagation involved both long projecting fibres and local intersegmental connections. These results suggest that the mammalian spinal cord contains propriospinal pathways subserving a metachronal transmission of motor information and that normally it may be involved in coordinating various parts of the body. The simple model developed here could be useful in unravelling more general mechanisms of neuronal circuit coupling.

(Received 21 March 2005; accepted after revision 3 August 2005; first published online 4 August 2005)
Corresponding author J.-R. Cazalets: CNRS UMR 5543, Université de Bordeaux II, Zone nord Bat 2, 2e étage, 146, rue Léo Saigna, 33076 Bordeaux cedex France. Email: jean-rene.cazalets@umr5543.u-bordeaux2.fr

The adequate functioning of the central nervous system requires that the various areas of the body operate together. For example, quadrupedal as well as bipedal locomotion is a complex motor behaviour which requires the simultaneous activation of most body parts including the trunk and neck, forelimbs, hindlimbs and tail. On this basis therefore the anatomical specialization of body parts involved in movements should be reflected at the neuronal level. However, the mammalian spinal cord should not be considered as an homogeneous chain of equipotent networks, as is the case for example in organisms which only exhibit anguilliform locomotion such as lamprey (Cohen, 1987; Mcclellan & Hagevik, 1999; Miller & Sigvardt, 2000; Grillner & Wallen, 2002), and *Xenopus* tadpoles (Roberts *et al.* 1998; Soffe *et al.* 2001; Tunstall *et al.* 2002). Rather, it should be considered as an interconnected ensemble of different neuronal subsets. What are the central mechanisms responsible for coordinating such distributed network activity and to what extent does coupling arise at the spinal level?

Muscles of quadruped forelimbs and hindlimbs are activated by neuronal networks that are located in the cervical (Jovanovic *et al.* 1998; Ballion *et al.* 2001) and lumbar cord enlargements (Rossignol, 1996; Cazalets & Bertrand, 2000*b*). Between these two regions (and also merging with them), are networks that drive motoneurones innervating trunk muscles along the axis of the body. Rhythmic activation of trunk muscles coordinated with appendicular locomotor activity has been observed in man (Thorstensson *et al.* 1982), rat (Gramsbergen *et al.* 1999) and cat (Zomlefer *et al.* 1984), where it was proposed that such activity has a central nervous origin (Koehler *et al.* 1984). Although coordination between these subsets of neuronal networks must occur during expression of meaningful locomotor behaviour, to date little data are available on the 'metanetwork' functioning of the spinal cord during ongoing locomotion.

The present study was therefore undertaken to address the functioning of the spinal cord, studying it as a whole, rather than as separate elements, and to see how its various regions might interact to coordinate motor activity. To this end, simultaneous multisite extracellular recordings were performed at the thoracic, lumbar and sacral levels in an isolated spinal cord preparation of newborn rat. Based on a method initially used by others (Bracci *et al.* 1996*b*), a pharmacological approach involving bath application of inhibitory synaptic blockers strychnine

 DOI: 10.1113/jphysiol.2005.086850

and bicuculline was employed for several reasons: (1) powerful and stereotyped bursts of action potentials are spontaneously produced; (2) the sharp onset of the bursts allows accurate determination of their timing; (3) the suppression of inhibitory connections within the spinal cord reveals underlying connectivity. It was therefore postulated that motor output recorded under these restrictive conditions might reveal coupling and other hard-wired properties of the system. Our results show that motor activity propagates along the spinal cord with a specific temporal pattern and that there is an asymmetry in the propagating characteristics from rostral to caudal *versus* caudal to rostral directions. Moreover, it was found that intersegmental coupling relies on a combination of local circuit connectivity as well as long projection fibres. This preparation offers a simplified model for studying network interactions in the mammalian nervous system.

Methods

Experiments were performed on isolated spinal cord preparations ($n = 25$) obtained from newborn Wistar rats, aged 0–3 days. Animals were anaesthetized by hypothermia, decapitated and then eviscerated in cold (4°C) oxygenated saline. The protocol was approved by the local ethics Committee of the University of Bordeaux 2 and was also in accordance with NIH guidelines. The experimental procedure used to prepare the spinal cord was as previously described in detail (Sqalli-Houssaini *et al.* 1991). The superfusion saline, bubbled with 95% O_2–5% CO_2, was composed as follows (mM): NaCl 130; KCl 3; $CaCl_2$ 2.5; $MgSO_4$ 1.3; NaH_2PO_4 0.58; $NaHCO_3$ 25; glucose 10, adjusted to pH = 7.4 with HCl. In order to minimize variability in axonal conduction speeds, the bath temperature was maintained between 24 and 26°C throughout all experiments. Spinal cords were sectioned at the T1 level at the beginning of the experiment.

All drugs were from Sigma. Strychine (Stry) and bicuculline (Bic) were freshly prepared and dissolved in the saline at the appropriate concentration. The mixture of Stry–Bic was bath-perfused throughout the experiment. Spontaneous activity, which generally started within 15 min following superfusion onset, was recorded continuously in sequences lasting 30 min. In some experiments, synaptic activity was suppressed using a modified saline from which Ca^{2+} was removed and 2 mM MnCl was added (phosphate was also removed from the saline to avoid precipitation).

Compartmentalization of the spinal cord was achieved by building walls of Vaseline, which was deposited across the bath and the cord with a fine syringe needle (0.5 mm). The water-tightness of walls was checked by over-filling one compartment on either side of a wall. If no change in the saline level occurred after several minutes, the walls were taken to be watertight. Mechanical cord lesions were performed using sharp MC-52 scissors (Moria, Paris).

Data acquisition was performed at 1 kHz on 16 channels using a Digidata 1322A interface driven by Axograph software (Axon Instruments). Up to 16 ventral roots were recorded simultaneously (Fig. 2), using stainless-steel pin electrodes (200 μm diameter) insulated from the bath with Vaseline (in all figures, the location of the extracellular electrodes has been indicated with dots). Signals, amplified 5000 × using laboratory-made amplifiers, were treated and analysed using Axograph analysis plug-ins. The signal was rectified without any smoothing or filtering. Each burst of activity was detected using a threshold value that was defined at 20% of the maximum amplitude for each trace and a minimum period value (according to the mean period in the measured sequence) was used in order that each burst could not be detected twice. Each time a burst was detected in this reference trace, it was sampled with all other associated recorded traces. Individual cycles were superimposed and then averaged (see Fig. 5). This process allowed the switch from a continuous mode of recording to an episodic one. The aim was to increase the signal-to-noise ratio in order to obtain a more accurate detection of burst onsets. Subsequent measurements were automatically performed on the averaged trace using a method based on onset detection (onset at 5% of maximum peak amplitude). Only the initial onset of burst activity was considered. Lag graphs were plotted using Igor-Pro software (Wavemetrics, OR, USA). Electrical stimulations were also performed with bipolar stainless-steel pin electrodes insulated with Vaseline.

Statistical analyses were performed on raw data. Fitting of the data by a Poisson distribution was made using a Kolmorov-Smirnov post test (Statistica, Statsfoft, OK, USA). The significance threshold was taken to be $P < 0.05$ (unless otherwise specified). Other analyses (linear regression, correlation and one-way ANOVA) were performed using Prism software (Graphpad software, CA, USA). For slope comparison, the Prism software used a method equivalent to an analysis of covariance (ANCOVA). Whenever the one-way ANOVA gave a significant result, all pair-wise comparisons were performed using the Tukey test. All data values in the text are means ± S.E.M.

Results

Spontaneous motor activity in the isolated cord

Bath application of strychinine and bicuculline at standard concentrations of 10^{-6} M and 2×10^{-5} M, respectively (Bracci *et al.* 1996*b*), induced repetitive bursts of action potentials, as shown in Fig. 1*A*. The mean period of 76 ± 11 s ($n = 13$ preparations) was in the same time range as that reported in previous work using the same protocol (Bracci *et al.* 1996*a*,*b*; Ballerini *et al.*

1997). A burst was identified by an abrupt onset of spiking activity as shown in the insets in Fig. 1*A*, which present two burst examples on a faster time base. Comparable effects were observed at concentrations ranging from 4×10^{-6} to 4×10^{-5} M bicuculline and 10^{-6} to 10^{-5} M strychnine, although with a longer interburst interval at the lowest bicuculline concentrations. To assess whether burst occurrence followed a specific temporal organization, burst distribution with time was analysed during sequences that lasted 100 min. Correlation analysis showed that there were no significant changes ($P = 0.95$) of the motor period with time, and a linear regression was performed (period duration *versus* recording time, slope 0.06) to fit the data (Fig. 1*B*). The number of burst occurrences during intervals of 1 min was also measured in sequences ranging from 60 to 120 min. The distribution of this burst occurrence was significantly ($P < 0.05$) fitted by a Poisson distribution as seen in the case experiment of Fig. 1*C* where the black line traces the theoretical distribution and the grey bars the actual distribution of motor burst period (Fig. 1*C*). The same significant result was observed in all 12 preparations examined (with a mean of 44 counted periods in each experiment). This therefore indicates that despite repetitive burst production, this activity occurred randomly under the experimental conditions.

Multiple simultaneous recordings along the intact spinal cord (Fig. 2*A*), always revealed a strict 1 : 1 relationship between all segments, i.e. when one segment was active there was always concommitent activity in the remaining ones (Fig. 2*B*; $n = 19$). However, a faster time scale (Fig. 2*C*), showed a distinct lag between motor bursts recorded at different spinal levels. In Fig. 2*C*, for example, the vertical dashed line indicates the onset of the first motor burst in the recorded sequence which, in this case, occurred at the high thoracic level with a rostro-caudal lag between remaining bursts.

The occurrence of an intersegmental delay was observed in all preparations ($n = 19$) in which spontaneous activity was expressed under bath application of Stry–Bic. Surprisingly, however, the locus at which a burst first occurred varied from one cycle to another as seen in Fig. 3, following analysis of the entire sequence monitored at a slow time scale in Fig. 3*A*. Figure 3*B* presents expanded views of three cycles (numbered from 1 to 3) extracted from the sequence. In all examples, the dashed line indicates the onset of the first motor burst. Cycle 1 (Fig. 3*B*1) started at the high thoracic level, cycle 2 (Fig. 3*B*2) was initiated at the lumbar level and cycle 3 started at the Co1 level. Moreover, during a given sequence, cycle initiation switched randomly from one site to another. In a further analysis of 386 cycles from nine preparations (Fig. 3*C*),

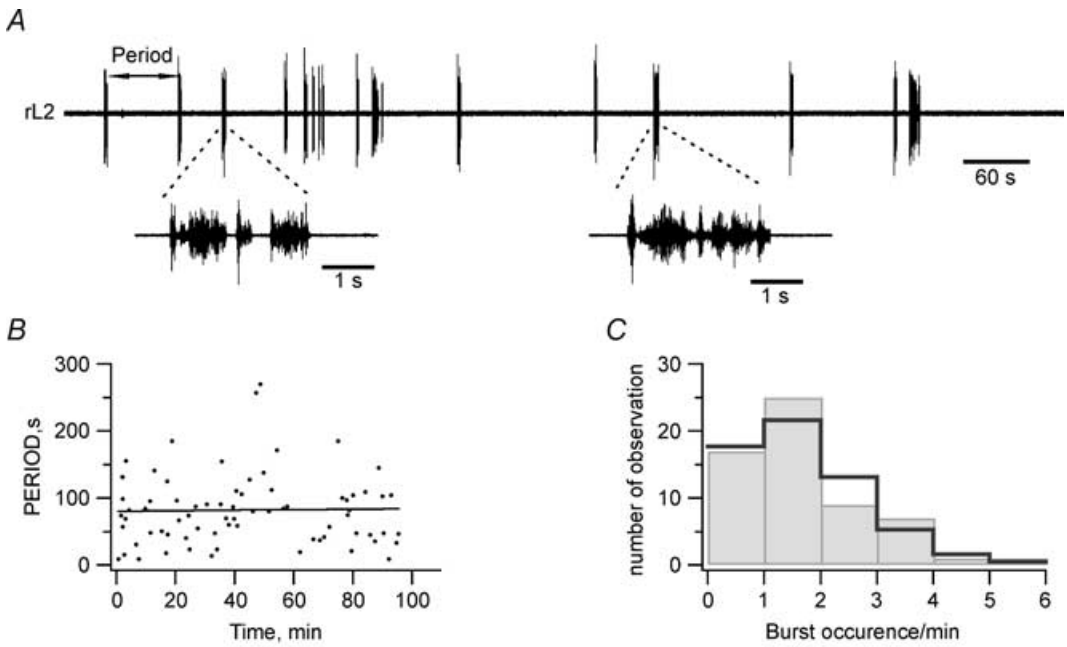

Figure 1. Characterization of spontaneous strychinine–bicuculline-induced bursting activity in the isolated neonatal rat spinal cord

A, extracellular recording from the second right lumbar ventral root (rL2). *B*, plot of motor burst period (time between 2 successive bursts) *versus* time during a 100 min recording sequence. The horizontal linear fit ($r = 0.02$) indicates that there was no change in burst period with time. *C*, burst period distribution; grey bars in the plot correspond to the number of observations (*y* axis) made for each category (*x* axis) per time unit. Black line indicates theoretical Poisson distribution.

the occurrence of cycle-initiating bursts was assigned to one of seven arbitrarily defined regions of the cord (*x* axis in Fig. 3*C*). The probability for initial burst occurrence was highest in three main cord regions (highlighted in grey in the spinal cord schema of Fig. 3*C*); namely the coccygeo-sacral area, the rostral lumbar/distal thoracic area and the rostral thoracic area. Thus, although the 'leading segment' could vary from one cycle to another, there were preferential areas in which bursting initiation occurred.

Since cross-inhibitory connections are abolished by Stry–Bic, the question arises as to whether the ipsi- and contralateral spinal cord exhibit equivalent capacities for burst initiation and propagation (3 experiments; Fig. 4). To assess this, simultaneous recordings of 14 ipsi- and contralateral ventral roots were performed. This revealed that the segmental lag did indeed occur on both sides of the cord (Fig. 4*A* and *B*), although bursting could be initiated either concomitantly in bilateral segments (as for example in the L2 segment in Fig. 4*A*) or with a delay on the contralateral side (Fig. 4*B*).

Recordings such as in Fig. 3*B*, provided the first indication that the intersegmental delay was not the same along the spinal cord. To investigate this further, averaged measurements were made of segmental delays at different cord levels. As shown in Fig. 5, the raw recordings of two ventral roots (Fig. 5*A*), were rectified (Fig. 5*B*1) and each motor burst was individualized with a selected segment taken as the reference (Fig. 5*B*2, see Methods for details). However, the variability in motor burst initiating site (see Fig. 3), made it impossible to pool all cycles from a given sequence. Therefore burst sequences were first categorized according to burst initiation locus in order to allow averaging of the traces (as illustrated in Fig. 5*B*3). The onset (grey trace in Fig. 5*B*3) was then measured for each segment from the averaged traces. For all traces, intersegmental lag was calculated as shown in Fig. 5*B*3 with respect to the leading burst that occurred amongst the 16 traces, then lag diagrams were plotted in which the first active ventral root was taken as zero. As observed in Figs 2–4, it was clear that the latencies were not randomly distributed and although this method resulted in a lost of information concerning the jitter in latency from burst to burst, it allowed a description of the overall property of motor burst propagation. For the sake of clarity a visual presentation was used in which the lag graph was plotted with the segment name given on the *y* axis and the associated delay on the *x* axis. The lag graph presented in Fig. 6*A* was obtained from two experiments in which bursting was initiated at the high thoracic (circles) or coccygeal (triangles) levels. Data pooled from seven experiments are also presented in Fig. 6*B*. A correlation analysis was performed by allocating a number from 1 to 23 to each segment; alternatively this could have been done as a function of distance since the length of one segment was around 1 mm. There was a systematic and significant change in the latency with distance within single experiments (Fig. 6*A*, $P < 0.001$) as well as for the overall set of data (Fig. 6*B*, $P < 0.0001$ $r = 0.83$). Inspection of these lag diagrams revealed two main properties of the intersegmental propagation of motor burst activation. First, there was a clear non-linearity in the propagation. The delay between each segment, and therefore the speed of propagation, was always shorter in the thoracic segments

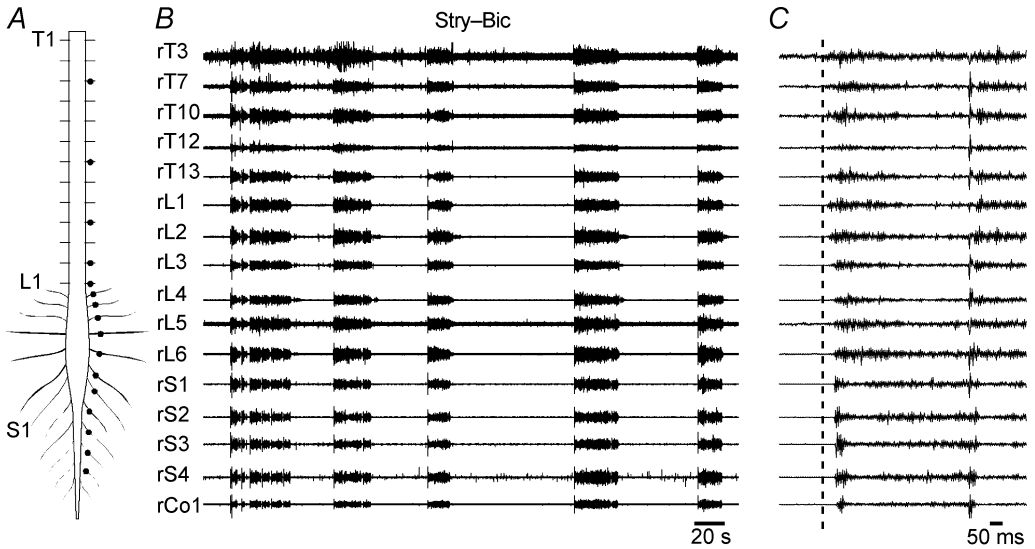

Figure 2. Multi-site ventral root recordings in the isolated spinal cord
A, diagram of the experimental preparation showing 16 recording sites at the thoracic, lumbar, sacral and coccygeal levels. T, thoracic; L, lumbar; S, sacral; Co, coccygeal. *B*, spontaneous motor bursts recorded during bath application of a mixture of strychnine and bicuculline. *C*, expanded view of the onset of a motor burst sequence.

than in the lumbar and coccygeal areas whatever the initiation site (caudal or rostral). This is further evident from the linear fits added to Fig. 6*B* (dashed lines) where pronounced changes correspond to changes in the speed of propagation along the spinal cord. Moreover, these data revealed regional significant differences ($P < 0.0001$) in propagation velocity that were more pronounced in the ascending than descending directions (see slope values in legend of Fig. 6 and in summary graph of Fig. 8*C*). The second important feature was the asymmetry in the total propagation time when comparing rostro-caudal *versus* caudo-rostral propagation. When starting caudally

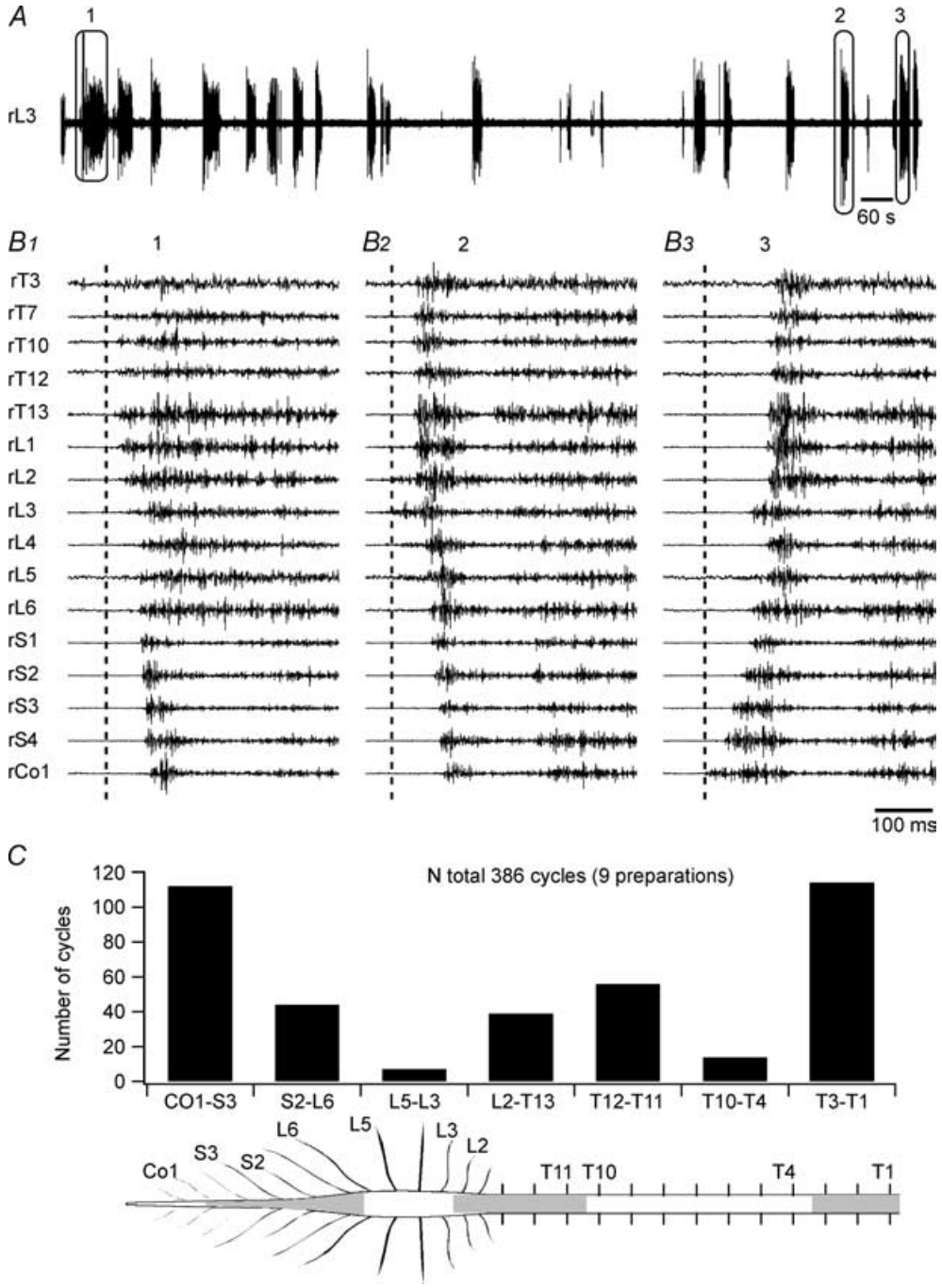

Figure 3. Spontaneous motor bursts are initiated at different segmental levels
A, single slow time-base recording from the right lumbar ventral root. *B*, expanded view of three cycles (1, 2 and 3) indicated in *A* and monitored on 16 ventral roots. In *B*1 the activity was initiated at the thoracic level, in *B*2 at the lumbar level and in *B*3 at the coccygeal level. *C*, plot of the number of spontaneous cycles generated at various spinal levels and diagram of the spinal cord indicating the zones (in grey) in which burst cycles were preferentially initiated.

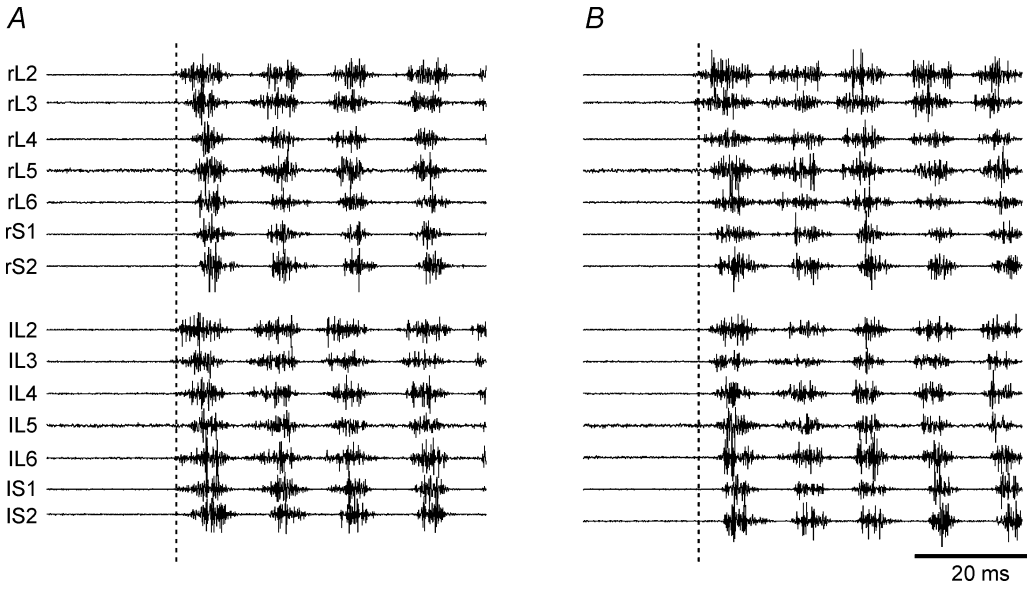

Figure 4. Bilateral onset of metachronal waves
Sequential propagation of activity could either occur concomitantly on both sides of the cord (*A*, starting simultaneously in right and left L2) or unilaterally (*B*, starting in left L2).

at the sacrococcygeal level, the motor wave reached the rostral end within a mean delay of 150 ± 11 ms, $n = 7$, while when starting rostrally at the thoracic level it took almost 80 ± 8 ms, $n = 7$, to reach the caudal end (Fig. 6*C*, upper two bars). Moreover, ascending waves reached the middle of the spinal cord (T13) within 130 ms while the descending one reached mid-cord in 20 ms (middle bars in Fig. 6*C*). Finally, the two waves crossed at the S2 level

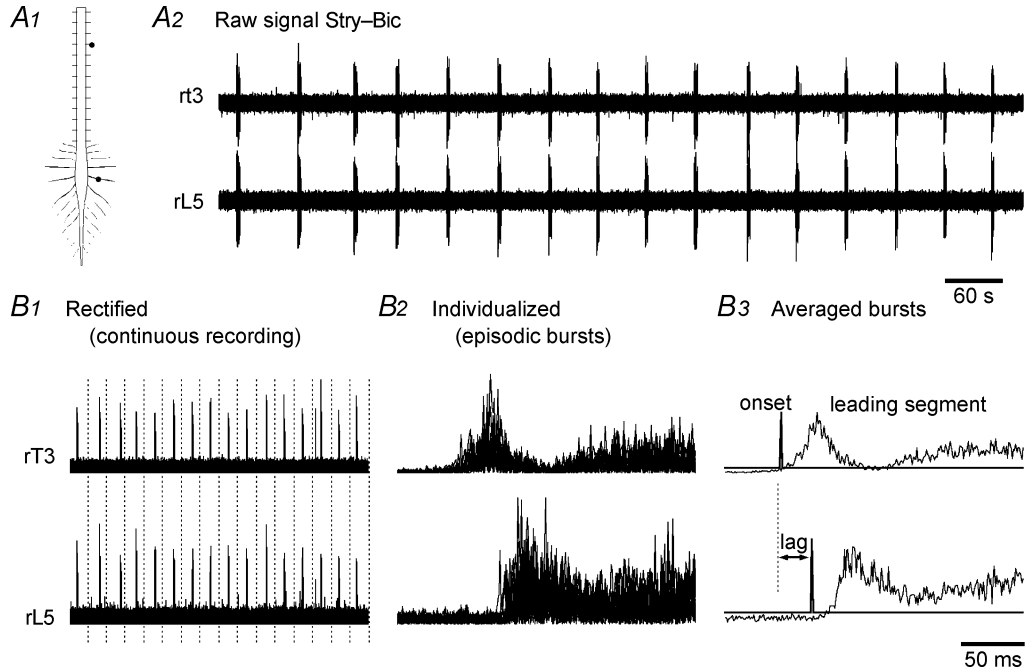

Figure 5. Analysis of Stry–Bic-induced bursts of action potentials
A, diagram of the experimental preparation (*A*1) and sample simultaneous recordings from two ventral roots (*A*2). *B*, bursts were rectified (*B*1), then each cycle was identified and the episodes were superimposed (*B*2) to obtain an averaged burst (*B*3). Dashed lines in *B*1 indicate how bursts were individualized. Alignments were based on the onset detection of a reference trace (here rT3). For each trace the onset of a burst was calculated and the lag to a different root burst was measured, taking the leading segment burst as zero.

within about 60 ms (lower bars in Fig. 6*C*). From this we calculated that the mean delay between each thoracic segment was around 2 ms under all conditions. It is also noteworthy that in some sequences, the activity did not propagate entirely sequentially along the spinal cord: in some instances distant segments fired concomitantly (arrows, Fig. 6*A*), and in the filled triangle preparation, for example, the L5 segment was activated posterior to more rostral segments during the ascending wave. Similarly, in the open circle preparation, the descending activity in the L6 segment started before the L4 and L5 segments. This could also be observed in raw recordings, as for example in

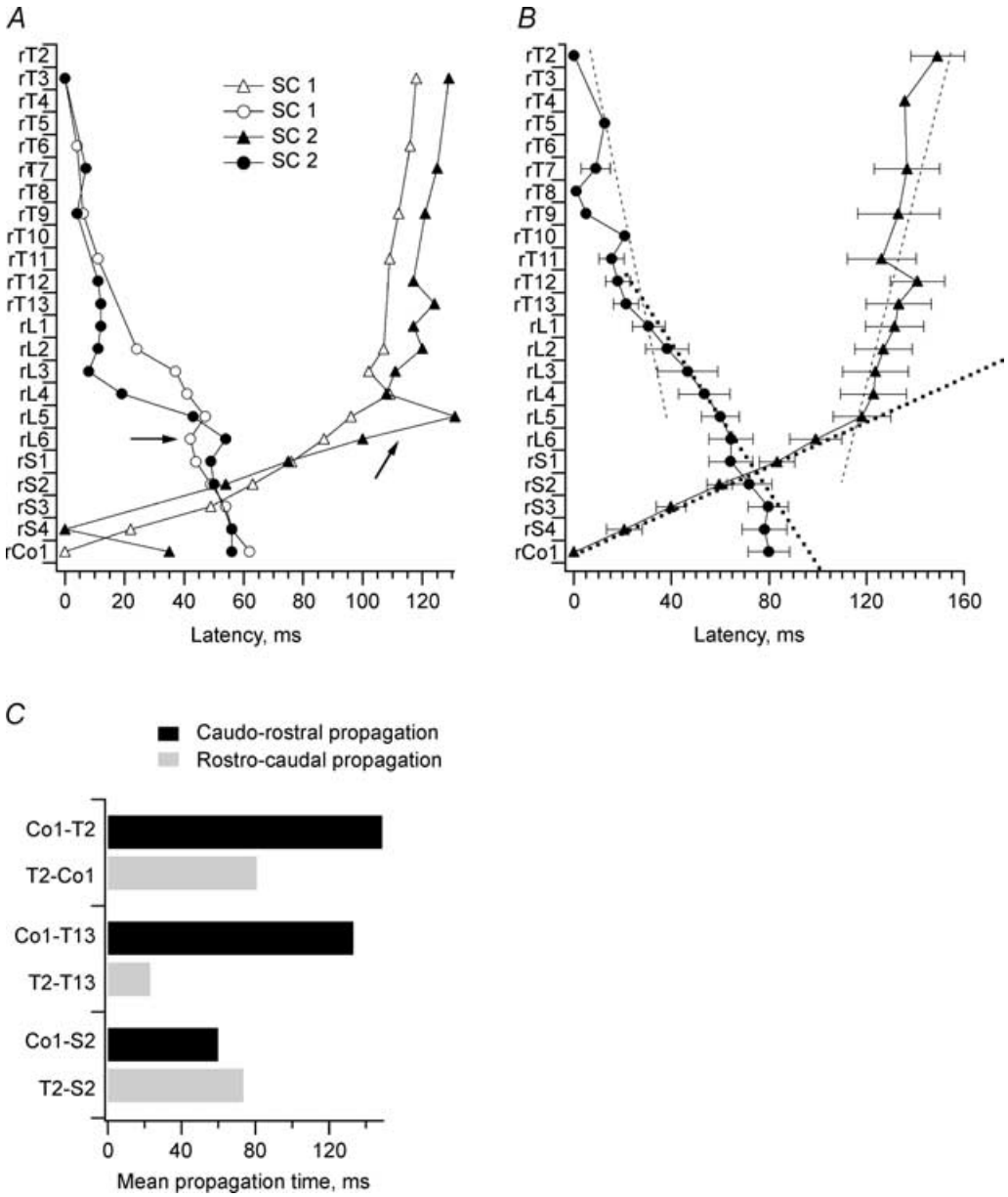

Figure 6. Lag diagrams of ascending and descending burst waves during Stry–Bic-induced activity
A, each curve presents lag values measured in 2 experiments. Open and filled symbols correspond to two different spinal cord preparations (SC1 and SC2) during rostro-caudal (circles) or caudo-rostral (triangles) propagation of burst waves. Arrows indicate anomalous timing in the curves (see text). *B*, mean lag diagrams obtained by pooling data from 6 experiments. Dashed lines correspond to the linear fit performed on two different regions of each curve. *C*, plot of the latency at various segmental levels during caudo-rostral (black) or rostro-caudal (grey) propagation. Error bars in *B* are S.E.M.s, the *y* axis indicates the segmental level and the *x* axis the latency from the initial burst in the cycle taken as the zero. Absolute slope value: 0.9 m s^{-1} (caudo-rostral propagation) and 0.6 m s^{-1} (rostro-caudal propagation) for thoracic T2–T13 region; 0.1 m s^{-1} (caudo-rostral propagation) and 0.2 m s^{-1} (rostro-caudal propagation) for the T13–Co1 region. The slope value expressed in m s^{-1} assumes that the length of each segment is 1 mm.

Fig. 3*B*3 where the L3 segment was active before the L4 and L5 segments. However, such apparent anomalies occurred more frequently in the S1–L5 area.

Mechanisms of intersegmental coordination

Two hypotheses could explain the propagation of motor activity described above. First, long ascending/descending fibres-distributing collaterals at each segmental level could sequentially activate the motor groups distributed along the spinal cord. Second, the propagation could derive from locally interacting segmental networks that segmentally activate each other.

To assess these possibilities, the rostral (T1) and caudal (Co2) parts of the spinal cord were stimulated electrically to test the potential implication of long spinal tracts and to measure the propagation velocities of any such direct pathway. To be sure that the activated pathways directly reached a given segment, without intervening synaptic relay, stimulations were performed under synaptic blockade (superfusion of 0 Ca^{2+} saline containing Mn^{+}, see Methods) in a compartmentalized spinal cord (Fig. 7*A*; $n = 4$ preparations). Electrodes for stimulation were placed at the rostral (T1) and caudal (Co2) ends of the spinal cord and ventral roots at lumbar and sacral levels were recorded (see dots in Fig. 7*A*). Under control conditions (note in the absence of Stry–Bic), stimulation at T1 elicited segmental bursts of action potentials with an increasing rostro-caudal delay (dashed lines, Fig. 7*B*1). Similarly, a caudo-rostral burst delay was observed from the S2 to L2 level when stimulating in Co2 (Fig. 7*C*1). Under bath application of 0 Ca^{2+}–Mn^{+} saline in the thoraco-lumbar compartment (including L2 rectangle; see Fig. 7*A*), stimulation at T1 no longer elicited a burst in the L2 ventral root (Fig. 7*B*2), indicating that the synaptic pathways to this caudal spinal region were blocked. However, a volley of action potentials was still recorded in the more caudal S1 and S2 unblocked

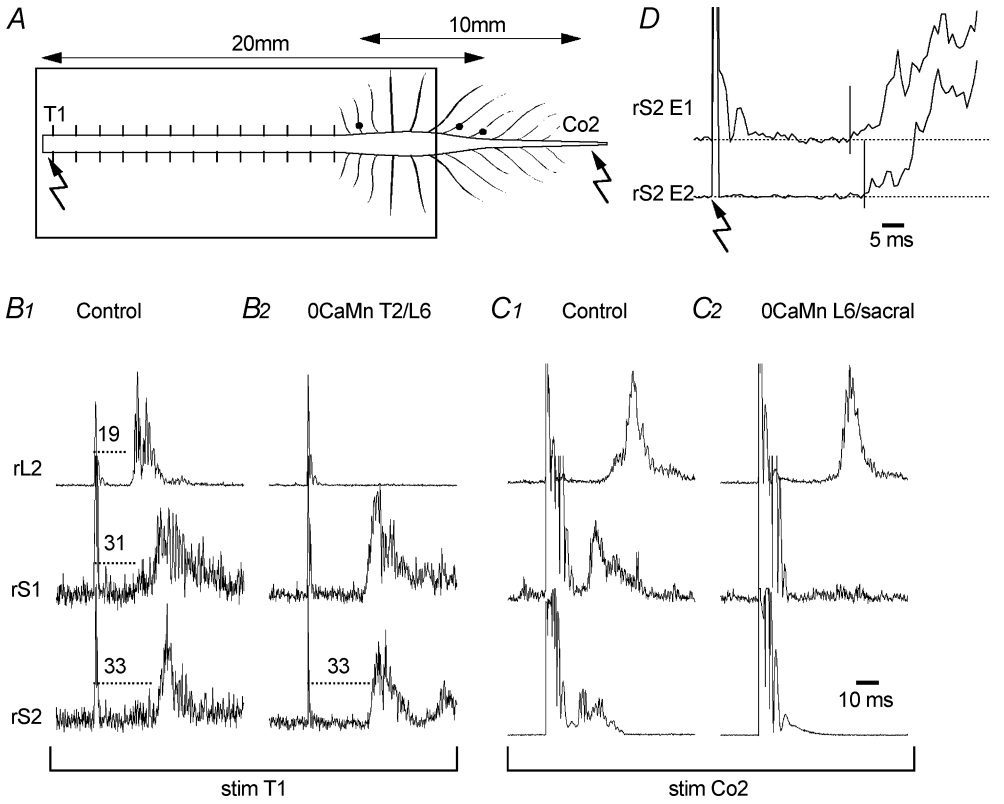

Figure 7. Evidence for segmental through-fibres spinal pathways
A, diagram of the experimental preparation. Bipolar stimulating electrodes were placed at the two ends (T1 and Co2) of the spinal cord. A Vaseline compartment allowed independent superfusion of the thoraco-lumbar (rectangle) and sacral areas. Spinal cord length is indicated. *B*, control rostral (T1) stimulation evoked a volley of action potentials in the 3 recorded caudal ventral roots (*B*1) during suppression of synaptic transmission by bath application of a saline containing 0 Ca^{2+}– Mn^{+} on the thoraco-lumbar area. Motor activity disappeared in L2 but persisted in sacral ventral roots (*B*2). *C*, activity recorded under control conditions during caudal (Co2) stimulation (*C*1) disappeared during suppression of synaptic activity in the caudal bath (*C*2) but persisted in the rostral bath. A single electrical shock (0.5 ms; 6 V) was applied in all cases. *D*, recording of sacral ventral root with 2 electrodes (distance between them, 4 mm) with a volley of action potentials elicited by stimulation (arrow) at the T1 level.

ventral roots with an unchanged latency. In a corollary experiment, synaptic activity was blocked in the caudal part of the spinal cord with the rostral compartment now placed under control saline (Fig. 7*C*2). Under these conditions, no activity was recorded in the sacral ventral roots in response to Co2 stimulation while activity was evident higher up the cord in the L2 ventral root (Fig. 7*C*2).

Axonal conduction velocity under these experimental conditions (25°C, 1 to 4 day-old rats) was estimated by recording a volley of action potentials (elicited by thoracic stimulation) with two recording electrodes placed on single sacral ventral root (distance 4 mm; Fig. 7*D*). The conduction velocity value established here (1.1 m s^{-1}) was similar to that calculated from intracellular recordings of antidromic axonal spikes elicited by extracellular stimulation (Fulton & Walton, 1986; Walton & Fulton, 1986). Altogether therefore, these data provide strong evidence that there are direct axonal pathways that run along the spinal cord, establishing connections at the different segmental levels.

In addition to the spontaneous expression and propagation of activity under Stry–Bic conditions (Figs 2–6), motor burst propagation was also examined when stimulating the spinal cord in the presence of strychnine and bicuculline. If electrical stimulation directly activates long fibres that distribute to each segmental level (see Fig. 7), it could be expected that such activity is propagated faster than that occurring spontaneously. In fact, if segmental activation involves long spinal fibres that distribute to each segmental level, it will be faster since it requires only the time for spike propagation along the fibres, as well as synaptic delay. According to the estimated conduction velocity in this preparation (around 1.1 m s^{-1}) and 2–3 ms for synaptic delay, the minimum time required for end-to-end propagation is about 30 ms which does not at all correspond to the propagation time (80–150 ms) recorded during spontaneous bursting (Fig. 6*B*). To test this possibility, stimulations were performed at three sites: T1 segment, L5 dorsal root and the Co2 segment. Figure 8 presents the corresponding lag plots obtained from the pooled data of six such experiments. The total time required for propagation was similar for ascending (triangles, 51 ± 5 s, $n = 6$) and descending (circles, 50 ± 9 s, $n = 6$) waves, and as predicted was much shorter than the propagation time observed during spontaneous activity (compare with Fig. 6*B*). The data values were compared for the total propagation time during spontaneous and stimulated conditions using a one-way ANOVA considering the four conditions, i.e. spontaneous rostro-caudal and caudo-rostral propagation, and rostro-caudal and caudo-rostral propagation during stimulation. It showed that the total time for propagation was not different

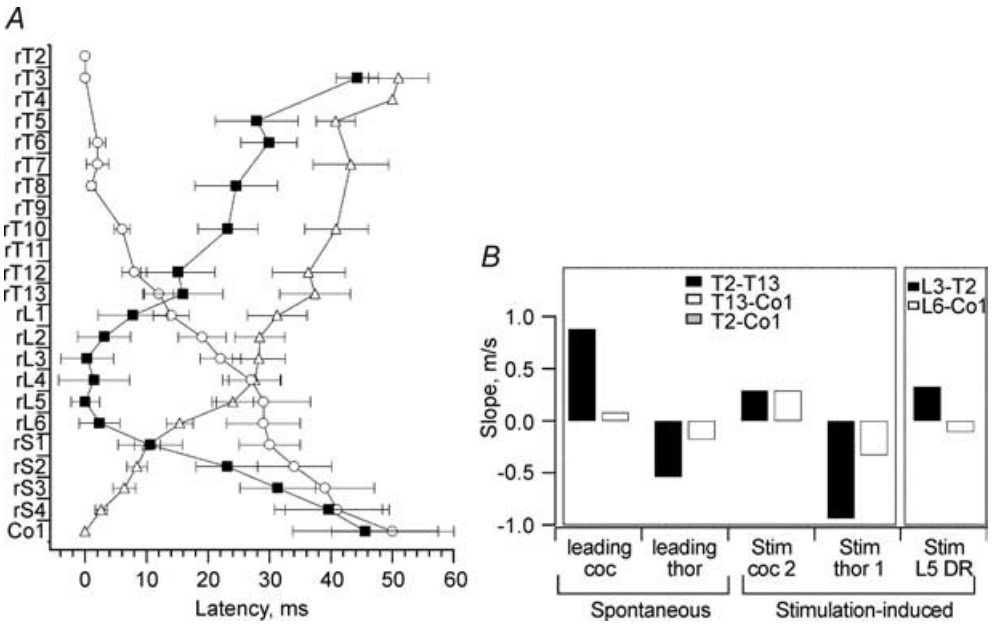

Figure 8. Intersegmental lags during spinal cord electrical stimulation
A, mean lag diagram after stimulation (1 shock, 0.5 ms; 3 V) of the rostral spinal cord (T1, ○), coccygeal area (Co2, △, or L5 dorsal roots (■). *B*, plots of lag slope during Stry–Bic-induced bursting (leading burst in either the coccygeal area (coc) or the thoracic area (thor)), during electrical stimulation of spinal cord (at Co2 or Thor1) and L5 dorsal root. The key panel above the histogram indicates the portion of curve on which the corresponding slope was calculated. The slope value expressed in m s^{-1} assumes that the length of each segment is 1 mm.

during stimulation in the rostro-caudal or caudo-rostral propagation directions, and that during stimulation the propagation was significantly faster than during spontaneous activity ($P < 0.005$). However, although the total propagation time was reduced, the lag plots established under electrical stimulation exhibited some similarities with spontaneous activity, with a change in the slope again seen from T2–T13 *versus* T13–Co1. In Fig. 8*B*, the slopes calculated from the lag diagrams of Figs 6*B* and 8*A* were plotted to compare lag changes during spontaneous and stimulation-induced propagation. As evident in Fig. 8*B* (left panel), slope values which were negative for descending and positive for ascending propagation, were always smaller during spontaneous propagation. Surprisingly, when stimulating the L5 dorsal root (line with filled squares in Fig. 8*A*), the ascending and descending waves emerging from mid-lumbar segments had a lower slope (Fig. 8*B*, right panel). Slope comparisons indicated that there was a significant difference ($P < 0.0001$) when considering the propagation in the T2–T13 segments (filled bars) to the propagation in the T13–Co1 segments (open bars). Altogether this suggests that dorsal root stimulation did not provoke the direct involvement of long fibre tracts but rather activated local networks via sensory input pathways, which in turn propagated the information up and down the cord with longer intersegmental delays.

Although the above data indicate that during spontaneous activity, local segmental interactions mediate motor burst propagation, Fig. 9 shows that long intersegmental pathways might also contribute to spontaneous burst propagation. In these experiments ($n = 3$), the spinal cord was separated into three compartments (see Fig. 9*A*1 and *B*1). Under control conditions, i.e. with Stry–Bic saline in all three compartments (Fig. 9*A*1), spontaneous motor bursts were observed in all recorded ventral roots. When the middle compartment (spanning 10 segments from T8 to L4) was bathed with a 0 Ca^{2+}–Mn^{+} saline, burst activity disappeared in the T13 ventral root. However, an absolute coordination persisted (all bursts crossed the 10 medial segments), between the segments above and below the intervening compartment, although the motor bursts were now weaker. Thus, this indicates that intersegmental coupling is indeed mediated in part by long projecting pathways which continue to propagate axial bursts in the absence of local interactions that were suppressed by the blockade of synaptic activity.

In a final step, lesion experiments were performed in an attempt to disrupt the long projection pathways implicated

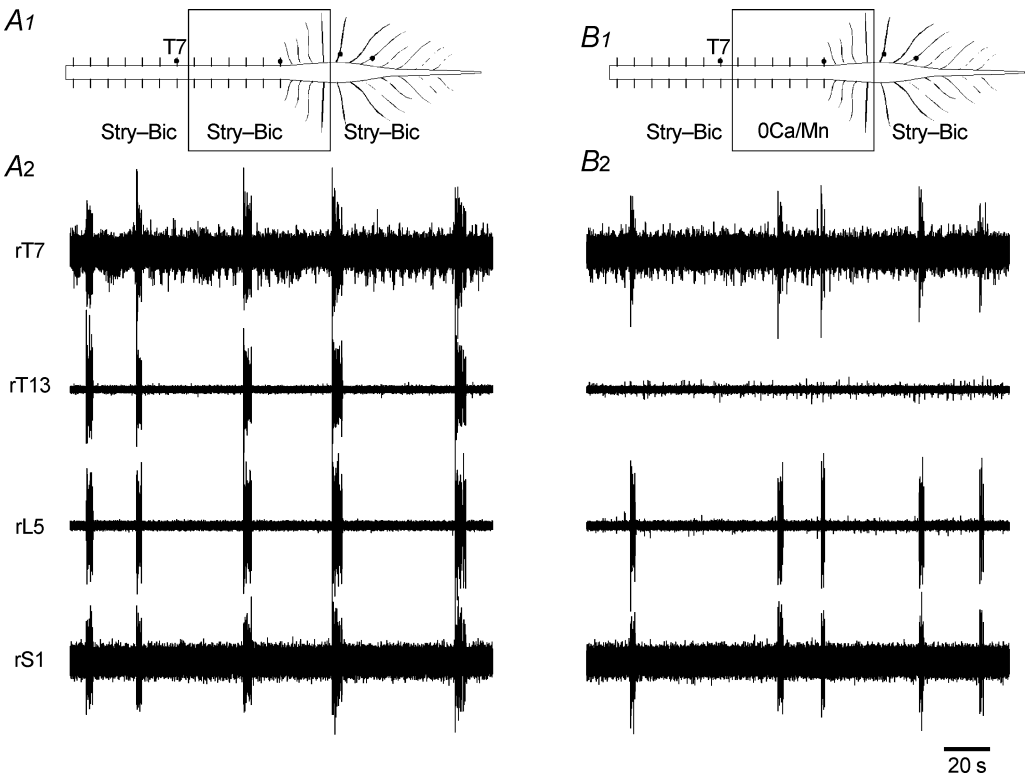

Figure 9. Involvement of long spinal tracts during spontaneous bursting
*A*1 and *B*1, diagram of the experimental preparation. *A*2, control activity recorded during bath application of Stry–Bic on entire preparation. *B*2, bursting in distant segments remained coordinated despite synaptic activity being blocked with 0 Ca^{2+}– Mn^{+} saline in the middle compartment.

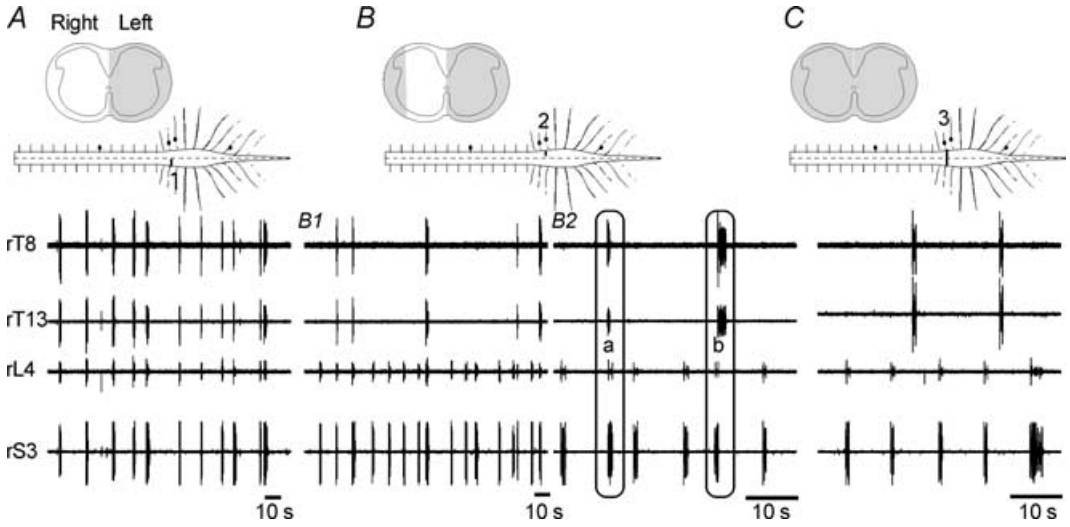

Figure 10. Changes in coupling after partial transverse sections of the spinal cord
Lesions at the L2–L3 junction were often gradually increased until axial coordination appeared to be modified. The top drawing of each panel indicates the extent of the cord lesion in the transverse plane (indicated in grey). *A*, motor activity recorded under bath application of Stry–Bic plus NMA, after contralateral cord section. *B*, lateral sectioning of the cord provokes a partial uncoupling between rostral and caudal activity and a change in the motor burst period. *C*, a complete section leads to total decoupling of the two sections of the spinal cord.

in this intersegmental coordination. In these experiments, an NMDA receptor agonist (NMA, 10^{-5} M) was added to the Stry–Bic saline to increase burst frequency (Bracci *et al.* 1996*b*) in order to observe sufficient bursts. It was found ($n = 5$ experiments) that under bath application of NMA, burst activity was still initiated in the three zones (as illustrated in Fig. 3), and did not markedly change the total time for propagation. Lesion sites are indicated on the spinal drawings of Fig. 10*A*–*C* (grey areas). In the six preparations tested under these conditions, a transverse section was first made on the side of the cord contralateral to the recording site. In a second step (Fig. 10*B*), a lateral section was made on the ipsilateral side. Following this lesion, the 1 : 1 coupling disappeared and the period of motor bursts changed (compare recordings at a slow time scale in Fig. 10*B*1); mean burst period decreased from 12 ± 2 s, $n = 6$ preparations, in control conditions to 40 ± 12 s in the rostral segments but was not significantly modified (11 ± 4 s) in the caudal spinal cord after the lesion. The two sections of the spinal cord were not, however, completely independently active. When a burst occurred in the rostral part, it was always coordinated with a burst recorded in the caudal part (see encircled activity in Fig. 10*B*2). Finally, when the spinal cord was completely sectioned (Fig. 10*C*), burst occurrence did not change further, but the two sections of the spinal cord were now independently active. These experiments therefore strongly suggest that sectioning the lateral white matter perturbs axial coordination, although unlesioned local circuit interactions may still ensure some longitudinal coupling.

Figure 11 summarizes our findings concerning the propagation of motoneurone burst activation in the isolated spinal cord of newborn rat. The largest circles indicate the three zones which were found, under the experimental conditions used, to be most active in initiating bursting (Fig. 3). Local interactions take place between each segment (double arrows)

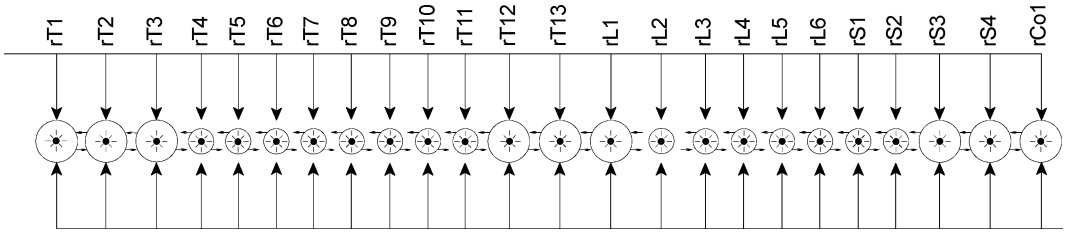

Figure 11. Schematic of the organization of spinal cord axial connections
Large circles correspond to zones of higher excitability. Ascending and descending through-fibre collaterals (large arrowheads) occur at the segmental level in parallel with local intersegmental connections (small arrows).

and long spinal fibres also ensure intersegmental coordination.

Discussion

Stry–Bic-induced motor activity

The bath application of strychnine and biculline has been extensively used to study motor rhythms *in vitro* (Ballerini *et al.* 1995, 1997; Bracci *et al.* 1996*a*,*b*, 1997, 1998). The idea is that such disinhibited motor networks express spontaneous burst patterns under these conditions. However, the disinhibition-induced bursting results not only from the specific activation of locomotor networks by removal of inhibition; both strychnine (Shapiro *et al.* 1974; Dale, 1995) and bicuculline (Debarbieux *et al.* 1998) block several types of K^+ and Ca^{2+} voltage-gated channels. Therefore, as shown in thalamic neurones (Debarbieux *et al.* 1998), it is likely that bursting induced by bicuculline and strychnine may result also from a synergistic action of both blockade of inhibition and of K^+ channels on various neuronal classes. The motor burst period values recorded here (mean 76 ± 11 s) were longer than those reported by Bracci *et al.* 1996*b*). This may be attributable to differences in extracellular K^+ concentration (3 mM in these experiments) which plays an important role in setting motor output (Sqalli-Houssaini *et al.* 1993; Bracci *et al.* 1998). It is unlikely that these motor rhythms are directly related to locomotion, and thus, inferences about bursting mechanisms under physiological conditions cannot be made. However, it is also clear that this method does allow inferences about some of the underlying wiring properties of the spinal networks in the absence of inhibition. The temporal analysis of motor bursting sequences also indicated that, under our experimental conditions, bursts were randomly emitted along the spinal cord, with their occurrence following a Poisson distribution (Fig. 1). Whatever the mechanisms for initial burst onset in a given cycle, which is presumably triggered by a summation of spontaneous excitatory synaptic activity, the multiple electrode recording method used here allowed disclosure of three zones of hyperexcitability in which burst initiation occurred preferentially (grey zones Fig. 3*C*2). First, the sacral area has recently been highlighted as having important rhythmogenic capabilities (Cazalets & Bertrand, 2000*a*; Lev-Tov *et al.* 2000), being implicated in tail movements (Gabbay *et al.* 2002). Second, it has been demonstrated that the low thoracic/high lumbar segments contain key rhythmogenic components for generating locomotor activity (Cazalets *et al.* 1995; see review by Cazalets, 2000). Finally, the third zone corresponds to the caudal end of the network driving forelimb movements (Ballion *et al.* 2001). These experiments therefore provide indirect confirmation of the heterogenous nature of spinal cord in terms of the longitudinal distribution of its rhythmogenic capacity.

Coupling mechanisms

Metachronal motor activity (one part being active after another) is a characteristic of all systems involving segmentally repeated muscles or appendages. This includes the locomotor systems of undulating animals such as fish (Cohen, 1987; Matsushima & Grillner, 1992; Miller & Sigvardt, 2000), tadpoles (Tunstall *et al.* 2002), snakes (Gasc *et al.* 1989), newt (Delvolve *et al.* 1997), leech swimming (Masino & Calabrese, 2002) as well as crayfish swimmeret beating (Skinner & Mulloney, 1998*b*). Metachronal activation allows the production of appropriately timed forces against the substrate to produce body displacement. Two main hypotheses have been raised to explain how these systems may work. On one hand long intersegmental neuronal tracts could be involved in coupling mechanisms while on the other hand, local interactions between adjacent segmental oscillators could explain the lag between segments (for review see Skinner, 1998*a*).

In one of the best studied systems, the lamprey spinal circuitry for locomotion, which is comprised of about 100 segments that are sequentially activated, the phase lag between consecutive segments remains close to 1% of the cycle, leading to approximately one wavelength of body curvature. In a recent study (Miller & Sigvardt, 2000; see also McClellan & Hagevik, 1999), the respective and complementary roles of the two mechanisms have been analysed. When blocking synaptic activity in a middle section of lamprey spinal cord preparation, segments rostral and caudal to the synaptically inactivated area remained coordinated, although the long coupling fibres were not able to maintain a correct phase lag across the blocked area. However, within these rostral and caudal sections of spinal cord, adequate local intersegmental phase lags were not changed by the loss of distant coupling inputs. Interestingly, comparable mechanisms may be operating in the rat spinal cord. This study has found that long projecting fibres also have access to distant segments (Fig. 7) since coordination persists when local connectivity is blocked (Fig. 9). On the other hand, if only long-distance coordinating fibres were involved, the total time for propagation would remain close to that encountered during direct stimulation of the ascending and descending pathways (i.e. 50 ms, open symbols in Fig. 8*A*) while the propagation time is in fact much longer during spontaneous (Fig. 6) or sensory-elicited motor burst activation (filled squares in Fig. 8*A*).

When partial sectioning of the lateral white matter was performed (Fig. 10*B*), the remaining pieces of the spinal cord above and below the lesion had different burst periods although relative coupling was maintained. These differences in motor period may be attributable to differences in the excitability of the segments. In the

lamprey spinal cord, it has been suggested that the motor period in distant segments may also be modulated by the relative complement between available shorter and longer coupling fibres (Miller & Sigvardt, 2000). Here, the changes in motor period seen after sectioning of the lateral spinal cord (Fig. 10) suggest that long fibres are necessary for maintaining appropriate timing of the overall network.

Despite similarities between rat spinal circuitry and the motor networks of invertebrate and lower vertebrate models, complete analogy does not occur. First, in the newborn rat spinal cord, the metachronal wave exhibits clear temporal discontinuities in that activity propagates faster in the rostral segments than in caudal ones (Fig. 6). It is unlikely that these region-specific changes in propagation rate are due to differences in conduction velocity or synaptic latency of long fibres, since activity propagates at the same speed in both directions during direct spinal cord stimulation (Fig. 8*A*). One explanation could be that in the rostral part of the cord, coordination relies more on long fibres coupling mechanisms while in the caudal section segmental interactions predominate. Alternatively, since the lumbar segments are intimately involved in hindlimb control, it could be that more complex local circuit interactions slow propagation through this region.

Besides propagation non-linearity, another striking characteristic of the newborn rat cord is the difference between spontaneous rostro-caudal and caudo-rostral propagation (Fig. 6), suggesting that there is a directional asymmetry in the functioning of the underlying circuitry. One possibility is that it could reflect the involvement of different neuronal networks in rostro-caudal or caudo-rostral directions of propagation. Again, in other models such as the lamprey, this is not observed under normal functioning of this system, although propagation in both directions may be observed when a middle segment is overexcited, relative to adjacent rostral and caudal ones (Matsushima & Grillner, 1992). In addition, differences in excitability between various zones found under our experimental conditions (Fig. 3*C*) have also been observed in the leech swimming system where the segmental oscillators are not uniform in their ability to generate rhythmic motor output (Hocker *et al.* 2000).

Although it is difficult to evaluate the respective contributions of local interactions *versus* long coupling pathways running along the spinal cord in the coordination process, it is likely that they may act simultaneously.

Functional relevance of intersegmental coupling

Locomotion as well as postural adjustments implicate the activation of motoneuronal pools along the body which subserve different functions. In this way, the task assigned to metachronal segmental activation in mammals does not fulfil the same function as in undulating animals. In the latter, the aim is to produce bending of the body that ensures adequate forces against the surrounding substrate. Although such a mode of coordination is not spontaneously exhibited in quadrupeds and man, it has been reported that there is metachronal activation of the axial musculature in man (Prince *et al.* 1994; J. R. Cazalets, unpublished observations). In mammals, trunk muscles have been shown to play a major role in postural maintenance since anticipatory postural adjustments are needed for a correct execution of movement. Besides this postural role, there is also a phasic activation of trunk muscles in synchrony with limb muscle activity during locomotion in various species including the cat (Carlson *et al.* 1979; Koehler *et al.* 1984; Zomlefer *et al.* 1984), rat (Gramsbergen *et al.* 1999) and man (Thorstensson *et al.* 1982). It is therefore likely that in mammals, a longitudinal coupling system may be involved in the axial and limb musculature.

In conclusion, the present data obtained in the presence of synaptic inhibitory blockers revealed that the newborn rat spinal cord possesses the intrinsic ability for the metachronal propagation of motor activity. Furthermore, these experiments highlight specific zones in the spinal cord with specific excitability and integration properties. It is proposed that the 'meta-network' which emerges under these conditions, may be at work in coordinating the various spinal regions during normal motor functioning associated with either postural or propulsive behaviours. It is now, however, necessary to perform further studies to see if normal network operation behaves in the same way. In any case the system described here may be used as a simple mammalian model for studying neuronal network coupling.

References

Ballerini L, Bracci E & Nistri A (1995). Desensitization of AMPA receptors limits the amplitude of EPSPs and the excitability of motoneurons of the rat isolated spinal cord. *Eur J Neurosci* **7**, 1229–1234.

Ballerini L, Bracci E & Nistri A (1997). Pharmacological block of the electrogenic sodium pump disrupts rhythmic bursting induced by strychnine and bicuculline in the neonatal rat spinal cord. *J Neurophysiol* **77**, 17–23.

Ballion B, Morin D & Viala D (2001). Forelimb locomotor generators and quadrupedal locomotion in the neonatal rat. *Eur J Neurosci* **14**, 1727–1738.

Bracci E, Ballerini L & Nistri A (1996*a*). Localization of rhythmogenic networks responsible for spontaneous bursts induced by strychnine and bicuculline in the rat isolated spinal cord. *J Neurosci* **16**, 7063–7076.

Bracci E, Ballerini L & Nistri A (1996*b*). Spontaneous rhythmic bursts induced by pharmacological block of inhibition in lumbar motoneurons of the neonatal rat spinal cord. *J Neurophysiol* **75**, 640–647.

Bracci E, Beato M & Nistri A (1997). Afferent inputs modulate the activity of a rhythmic burst generator in the rat disinhibited spinal cord in vitro. *J Neurophysiol* **77**, 3157–3167.

Bracci E, Beato M & Nistri A (1998). Extracellular K^+ induces locomotor-like patterns in the rat spinal cord in vitro: comparison with NMDA or 5-HT induced activity. *J Neurophysiol* **79**, 2643–2652.

Carlson H, Halbertsma J & Zomlefer M (1979). Control of the trunk during walking in the cat. *Acta Physiol Scand* **105**, 251–253.

Cazalets JR (2000). Organization of the spinal locomotor network in neonatal rat. In *Neurobiology of Spinal Cord Injury*, ed. Kalb R & Stritmatter Sm, pp. 89–111. Humana Press Inc., Totowa, NJ.

Cazalets JR & Bertrand S (2000*a*). Coupling between lumbar and sacral motor networks in the neonatal rat spinal cord. *Eur J Neurosci* **12**, 2993–3002.

Cazalets JR & Bertrand S (2000*b*). Ubiquity of motor networks in the spinal cord of vertebrates. *Brain Res Bull* **53**, 627–634.

Cazalets JR, Borde M & Clarac F (1995). Localization and organization of the central pattern generator for hindlimb locomotion in newborn rat. *J Neurosci* **15**, 4943–4951.

Cohen JR (1987). Intersegmental coordinating system of the lamprey central pattern generator for locomotion. *J Comp Physiol A* **160**, 181–183.

Dale N (1995). Experimentally derived model for the locomotor pattern generator in the *Xenopus* embryo. *J Physiol* **489**, 489–510.

Debarbieux F, Brunton J & Charpak S (1998). Effect of bicuculline on thalamic activity: a direct blockade of IAHP in reticularis neurons. *J Neurophysiol* **79**, 2911–2918.

Delvolve I, Bem T & Cabelguen JM (1997). Epaxial and limb muscle activity during swimming and terrestrial stepping in the adult newt, Pleurodeles waltl. *J Neurophysiol* **78**, 638–650.

Fulton BP & Walton K (1986). Electrophysiological properties of neonatal rat motoneurones studied *in vitro*. *J Physiol* **370**, 651–678.

Gabbay H, Delvolve I & Lev-Tov A (2002). Pattern generation in caudal-lumbar and sacrococcygeal segments of the neonatal rat spinal cord. *J Neurophysiol* **88**, 732–739.

Gasc J-P, Cattaert D, Chasserat C & Clarac F (1989). Proplusive action of a snake pushing again a single site: its combined analysis. *J Morph* **201**, 315–329.

Gramsbergen A, Geisler HC, Taekema H & Van Eykern LA (1999). The activation of back muscles during locomotion in the developing rat. *Brain Res Dev Brain Res* **112**, 217–228.

Grillner S & Wallen P (2002). Cellular bases of a vertebrate locomotor system-steering, intersegmental and segmental co-ordination and sensory control. *Brain Res Brain Res Rev* **40**, 92–106.

Hocker CG, Yu X & Friesen WO (2000). Functionally heterogeneous segmental oscillators generate swimming in the medical leech. *J Comp Physiol A* **186**, 871–883.

Jovanovic K, Cheng J, Yoshida K & Stein RB (1998). Localization and modulation of rhythmogenic locomotor network in the mudpuppy (Necturus maculatus). *Ann N Y Acad Sci* **860**, 480–482.

Koehler WJ, Schomburg ED & Steffens H (1984). Phasic modulation of trunk muscle efferents during fictive spinal locomotion in cats. *J Physiol* **353**, 187–197.

Lev-Tov A, Delvolve I & Kremer E (2000). Sacrocaudal afferents induce rhythmic efferent bursting in isolated spinal cords of neonatal rats. *J Neurophysiol* **83**, 888–894.

Masino MA & Calabrese RI (2002). A functional asymmetry in the leech heartbeat timing network is revealed by driving the network across various cycle periods. *J Neurosci* **22**, 4418–4427.

Matsushima T & Grillner S (1992). Neural mechanisms of intersegmental coordination in lamprey: local excitability changes modify the phase coupling along the spinal cord. *J Neurophysiol* **67**, 373–388.

Mcclellan AD & Hagevik A (1999). Coordination of spinal locomotor activity in the lamprey: long-distance coupling of spinal oscillators. *Exp Brain Res* **126**, 93–108.

Miller WI & Sigvardt KA (2000). Extent and role of multisegmental coupling in the Lamprey spinal locomotor pattern generator. *J Neurophysiol* **83**, 465–476.

Prince F, Winter DA, Stergiou P & Walt SE (1994). Anticipatory control of upper body balance during human locomotion. *Gait Posture* **2**, 19–25.

Roberts A, Soffe SR, Wolf ES, Yoshida M & Zhao FY (1998). Central circuits controlling locomotion in young frog tadpoles. *Ann N Y Acad Sci* **860**, 19–34.

Rossignol S (1996). Neural control of stereotypic limb movements. In *Handbook of Physiology*, Section 12, *Exercise: Regulation and Integration of Multiple Systems*, ed. Rowell B & Sheperd JT, pp. 173–216. American Physiological Society, Oxford.

Shapiro BI, Wang CM & Narahashi T (1974). Effects of strychnine on ionic conductances of squid axon membrane. *J Pharmacol Exp Ther* **188**, 66–76.

Skinner FK & Mulloney B (1998*a*). Intersegmental coordination in invertebrates and vertebrates. *Curr Opin Neurobiol* **8**, 725–732.

Skinner FK & Mulloney B (1998*b*). Intersegmental coordination of limb movements during locomotion: mathematical models predict circuits that drive swimmeret beating. *J Neurosci* **18**, 3831–3842.

Soffe SR, Zhao FY & Roberts A (2001). Functional projection distances of spinal interneurons mediating reciprocal inhibition during swimming in Xenopus tadpoles. *Eur J Neurosci* **13**, 617–627.

Sqalli-Houssaini Y, Cazalets JR & Clarac F (1993). Oscillatory properties of the central pattern generator for locomotion in neonatal rats. *J Neurophysiol* **70**, 803–813.

Sqalli-Houssaini Y, Cazalets JR, Fabre JC & Clarac F (1991). A cooling/heating system for use with in vitro preparations: study of temperature effects on newborn rat rhythmic activities. *J Neurosci Meth* **39**, 131–139.

Thorstensson A, Carlson H, Zomlefer MR & Nilsson J (1982). Lumbar back muscle activity in relation to trunk movements during locomotion in man. *Acta Physiol Scand* **116**, 13–20.

Tunstall MJ, Roberts A & Soffe SR (2002). Modelling inter-segmental coordination of neuronal oscillators: synaptic mechanisms for uni-directional coupling during swimming in Xenopus tadpoles. *J Comput Neurosci* **13**, 143–158.

Walton K & Fulton BP (1986). Ionic mechanisms underlying the firing properties of rat neonatal motoneurons studied in vitro. *Neuroscience* **19**, 669–683.

Zomlefer MR, Provencher J, Blanchette G & Rossignol S (1984). Electromyographic study of lumbar back muscles during locomotion in acute high decerebrate and in low spinal cats. *Brain Res* **290**, 249–260.

Acknowledgements

The author thanks S. Bertrand and J. Simmers for their valuable comments on the manuscript and for correcting the English. Many thanks to G. Barrault and M. Falgairolle for Axograph plug-in development. This work was funded in part by the Ministère de la Recherche (ACI Neuroscience), by the Région Aquitaine and by the DGA (Ministère de la défense no. 0334045).